MEASUREMENT OF THE SHAPE OF OXALATE CRYSTALS BY AUTOMATED OPTICAL IMAGE ANALYSIS

Bekker AV*, McShane J, Vassallo JD, Bedell D, Li TS, Livk I

CSIRO Process Science and Engineering, Parker CRC for Integrated Hydrometallurgy Solutions
PO Box 7229, Karawara WA 6152, Australia

Abstract

A new automated static optical image analysis (SOIA) method was developed for characterising the shape of sodium oxalate crystals by separately measuring their length and width. The automated SOIA technique combines crystal image acquisitioning with a custom-developed numerical algorithm for morphological analysis of crystals. The automation of the two main measuring steps enables characterisation of a large number of oxalate crystals ensuring statistically meaningful results. As part of the numerical algorithm, a rectangularity-based morphological filter was implemented to eliminate overlapping crystals and crystal networks. The developed optical sizing technique has a low detection limit of 0.25 µm, which is close to the theoretical resolution of optical microscopy. It is demonstrated that the new automated SOIA sizing technique is very sensitive in identifying oxalate crystals of different shape. The SOIA measured crystal size distributions were compared to those obtained by the AccuSizer sizing instrument to confirm that they were consistent with the measurements obtained by a conventional crystal sizing instrument.

1. Introduction

In alumina refineries around the world, sodium oxalate emerges as a common impurity that needs to be appropriately managed to ensure efficient and stable operation of the Bayer process. Commonly, 5-10% of the organic carbon, which mostly enters Bayer process liquors in the form of humic substances (Rao & Goyal, 2006), decomposes to sodium oxalate during the digestion stage (Lever, 1983; Grocott, 1988). When dissolved, sodium oxalate has no significant effect on precipitation yield or product quality (Power, 1991). However, through recycling of Bayer liquor the oxalate liquor concentration builds up resulting ultimately in precipitation of solid phase oxalate (SPO), which does affect the process in an undesirable manner (Sipos, 2001). Alcoa's nine refineries alone, for example, produce nearly 200 metric tonnes of SPO each day (Alcoa Newsletter, 2010). Sodium oxalate crystals in the Bayer precipitation circuit commonly exhibit an elongated needle-like shape as a result of different crystal growth rates of various oxalate crystal faces (Rehani *et al*., 1999). To enable an effective control of SPO in the Bayer process, it is essential to have available an accurate and efficient technique for characterisation of the size and shape of sodium oxalate crystals.

Measuring oxalate particle size by traditional methods, such as laser light scattering Malvern Multisizer or AccuSizer instruments, only provides information on the diameter of an equivalent sphere. Due to the irregular shape of SPO crystals, this information is insufficient, as it does not indicate anything about the crystal geometry. A 2-D sizing method, at least, is required in order to characterise crystal aspect ratio, and crystal length and width.

A 2-D technique for measuring crystal size was applied previously, for example, by Wang *et al*. (2006) using an optical microscopy in-situ dynamic image analysis approach. This method, which is also described by ISO 13322-2:2006 standard (2006), is mostly suitable for measurements in very dilute crystallisation systems with consistent and stable background. In addition, the in-situ 2-D imaging suffers from problems associated with the random orientation of irregular crystals in a 3-D space (Li *et al*., 2006). This can significantly distort actual dimensions of suspended crystals. To avoid some of these issues, a 3-D in-line digital holographic microscopy was developed for crystal characterisation by Darakis *et al.* (2010) and Khanam *et al.* (2011). However, this method is restricted by a minimum size limit of 4-10 µm due to the holographic diffraction effects becoming prominent at that crystal size. Although potentially very powerful, this technique is currently not suitable for measuring a large number of crystals, as required in the case of SPO.

To overcome some of the restrictions mentioned above, a new automated static optical image analysis (SOIA) based sizing technique for measuring a 2-D size of individual oxalate crystals was developed. The novel crystal sizing technique, which is based on the analysis of optical microscopy images of oxalate crystals, has a low detection limit of 0.25 µm, which is close to the theoretical resolution of optical microscopy. The automated SOIA technique combines tools for acquisitioning of optical images with a numerical algorithm for the morphological analysis of crystal images. The automation of the two main steps, image acquisitioning and image analysis, enables a rapid characterisation of a large number of oxalate crystals ensuring statistically meaningful results. As part of the newly developed numerical algorithm, a specialised morphological filter was designed to eliminate overlapping crystals and crystal networks.

In literature, three main types of image analysis algorithms for morphological separation of crystals are discussed. Firstly, model-based recognition algorithms compare measured crystal shape with a geometrical crystal model. It was shown that in the systems with uniform crystals a model-based algorithm SHARC (Larsen *et al*., 2006) can successfully identify overlapping elongated crystals. Secondly, statistical morphological algorithms were shown to be able to separate a desirable class of crystals from the whole crystal population using different morphological parameters (Ferreira *et al*., 2011). A combination of the first two morphological separation approaches was successfully applied in our development. Thirdly, neural network-based morphological separation algorithms, trained on a selected class of crystals, were also found to be able to identify and separate individual crystals from crystal networks (Zaknich *et al*., 1995), but were not implemented as part of our numerical algorithm.

In this work, it is demonstrated that the new automated SOIA technique for characterising size and shape of oxalate crystals is very robust and delivers statistically meaningful data. The optical image analysis-based measurements of a 1-D size of SPO crystals are validated against the crystal size distributions obtained by a commercially available AccuSizer sizing instrument.

2. Static Optical Image Analysis (SOIA)

The new SOIA methodology was applied to quantify the shape of three different types of needle-like oxalate crystals, prepared in the laboratory such to mimic properties of SPO crystals found in the plant.

In all cases, SPO samples were transferred onto a glass slide used to acquire optical microscopy images. The preparation of sample slides involved a number of steps. Firstly, a representative sample of oxalate needle-like crystals was suspended in a non-dissolving liquid. A small volume of crystal suspension was transferred onto a 2 × 8 cm glass slide, and placed in the oven to dry. Optical images of the dispersed crystals were acquired using a Nikon Eclipse Ti-E inverted optical microscope equipped with an automated motorized stage. A Nikon objective lens with 40x magnification and a high resolution 5 Mpix camera were used to achieve the optical diffraction limit of 0.2 µm. The Nikon DS-Fi1 CCD camera, with an image resolution of 2560 × 1920 pixels, was mounted on the microscope for image acquisitioning and digitization. An example of the acquired image with oxalate crystals is presented in Fig. 1(a).

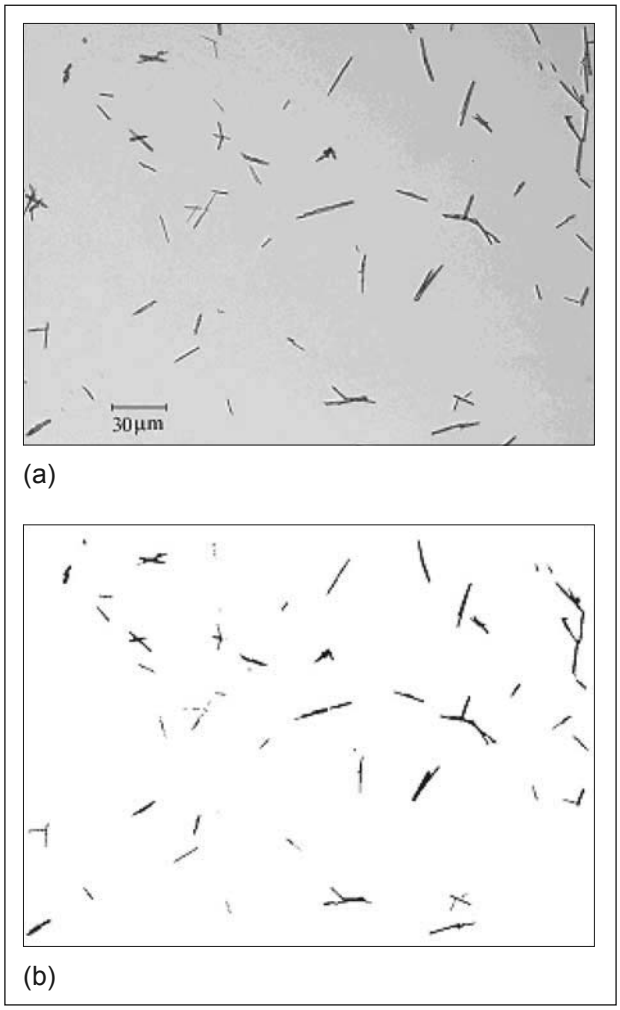

Fig. 1. Optical microscopy image (5 Mpix resolution) of needle-like oxalate crystals: (a) original digital image, and (b) binary image with the highlighted objects identified by the developed image analysis algorithm.

The image acquisitioning and pre-processing steps were controlled by Nikon's NIS-Elements software. Original digital images for a given sample of crystals were subsequently batch-processed using a custom-developed image analysis algorithm. Edges of crystals were detected through automatic threshold decomposition of the original gray-scale images. Any internal holes in individual crystals, detected in binary images, were automatically filled in. An example of the binary image is shown in Fig. 1(b), with the identified crystals shown in black. To obtain individual crystals, the objects identified in each image were morphologically analysed and filtered if necessary, as explained in the section below. Identified crystals were analysed for their projected area (*A*), and length (*L*) - the distance between the two furthest points on the crystal perimeter. Based on the primary morphological data, the crystal width (*W*) was estimated as the projected area divided by the length, as illustrated in Fig. 2(b). The morphological measurements were also used to quantify the crystal perimeter (*P*). It is important to note that crystals touching the image boundaries, as shown in Fig. 1(a), were excluded from the binary image, shown in Fig. 1(b), to avoid inaccurate crystal size measurements. Also crystals with circle equivalent diameter, *CED*, less than 0.5 µm were removed. The *CED* is defined as

$$CED = \sqrt{\frac{4A}{\pi}} \tag{1}$$

In the above equation *A* is the crystal projected area. The lower size limit, of 0.5 µm was chosen as an arbitrary size larger than the optical diffraction limit of 0.2 µm. In addition to the lower size limit, a specialised morphological filtration algorithm was applied to avoid measurement of overlapping crystals and crystal networks, resulting in a measurement of only individual crystals with close to rectangular shape.

3. Morphological filtering of crystals

To apply morphological filtering, the shape of needle-like oxalate crystals, shown in Fig. 1(a) and Fig. 2(a), was approximated by an ideal rectangular prism of length *L* and equal width and height of *W*. The volume of the approximated crystal is defined as $V_c=LW^2$.

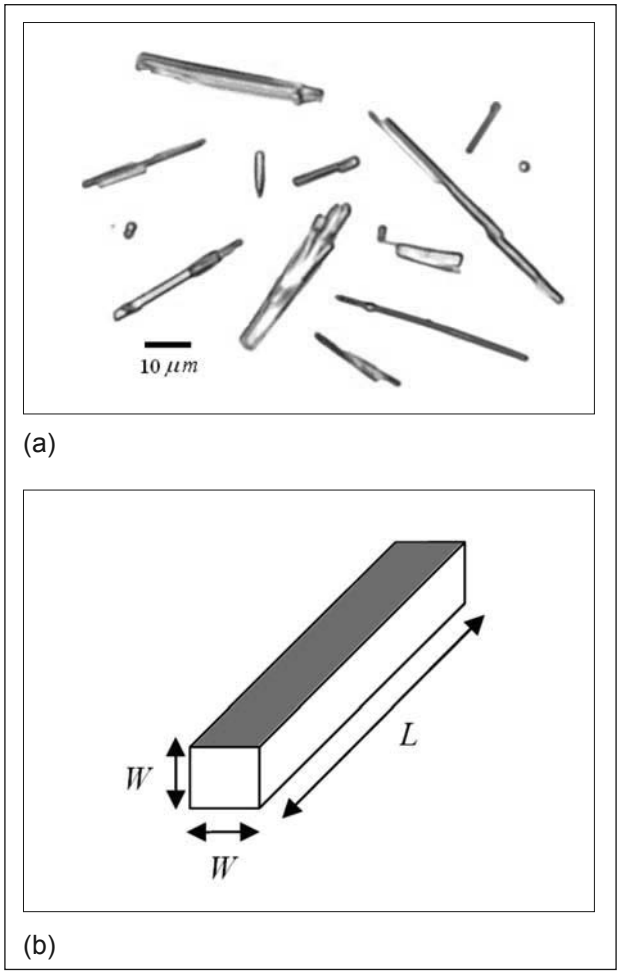

Fig. 2. An optical microscopy digital image, 40x magnification, of needle-like oxalate crystals (a), and a two-dimensional rectangular approximation of a 3-D crystal (b).

For the purpose of further discussion in this work, we define the crystal aspect ratio as

$$\text{Aspect Ratio} = \frac{W}{L} \quad (2)$$

As described in Bekker *et al.* (2011), the image analysis algorithm applies morphological filtering based on the evaluation of the rectangularity of identified image objects. The rectangularity-based morphological filter combines sensitivity of both "boundary-based" and "area-based" filters to detect thin boundary intrusions and networking crystals. By applying a selected threshold for the rectangularity filter it is possible to separate needle-like crystals from irregularly shaped objects, which are assumed to result from overlapping crystals and crystal networks. The developed rectangularity filter is non-dimensional and it can be applied for the identification of crystals of different size.

Image analysis results obtained using the rectangularity filter are illustrated in Fig. 3(a), which shows highlighted final identified oxalate crystals. When compared to the unfiltered binary image in Fig. 1(b), it can be noted that irregular objects are not present anymore due to the effect of filtering.

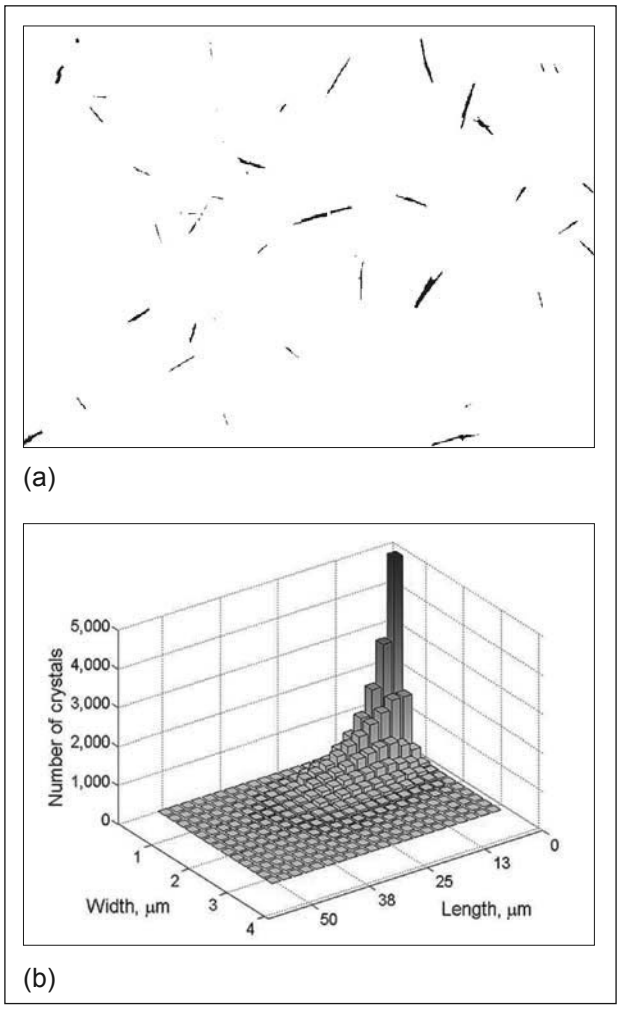

Fig. 3. Needle-like crystals identified after applying a non-dimensional rectangularity filter (a), and a complete 2-D size distribution of identified needle-like oxalate crystals (b).

One of the prepared oxalate crystal samples (SPO A) was analysed by processing 600 optical 5 Mpix images. Shown in Fig. 3(b) is the 2-D size distribution of oxalate crystals 'SPO A' obtained by analysing optical images using the procedure described above. The image analysis in this case resulted in 36,267 identified needle-like oxalate crystals from a total of 42,093 objects identified initially. The crystal rejection rate was 13.86%. According to the discussion in Bekker *et al*. (2011), the critical number of crystals, N_{crit}, required to ensure statistically meaningful data was estimated to be more than 10,000, the exact number pending on the shape of the actual distribution.

Reproducibility of the new image analysis technique, including sampling preparation, was tested using oxalate SPO A samples by repeatedly applying the developed image analysis procedure. 600 images were collected in each case to generate the data on a minimum of 32,000 individual needle-like crystals. Obtained oxalate crystal length and width number-based distributions for three samples of 'SPO A' crystals are shown in Fig. 4.

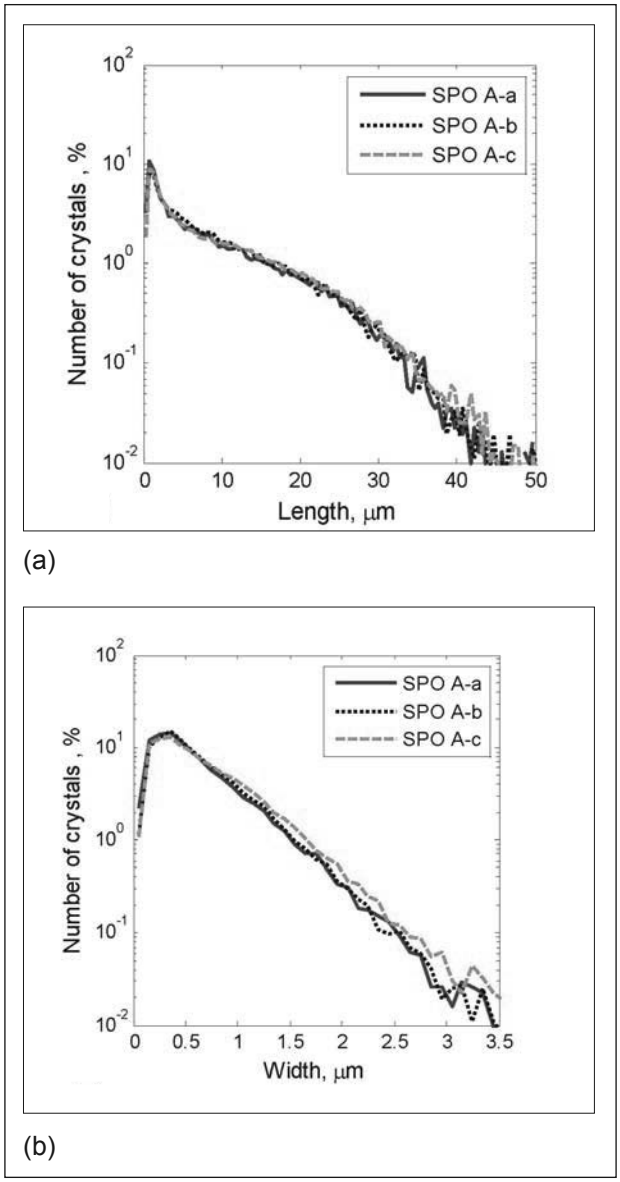

Fig. 4: Reproducibility of measured length (a) and width (b) distributions of 'SPO A' oxalate crystals.

The results shown in Fig.4 indicate highly reproducible measurements of a 2-D size of oxalate crystals. Note that the measurement uncertainties rapidly increase as the number of measured crystals drop below 0.1% of the maximum number of crystals.

4. Shape of different types of oxalate crystals

The developed image analysis methodology was applied to quantify shape distribution of three different types of oxalate crystals with the aim to verify the ability of the new image analysis technique to differentiate between different types of needle-like oxalate crystals.

Projected area-based size distributions, shown previously to be quite sensitive in revealing differences between different crystal types (Bekker *et al*., 2011), are used to present measured data. Presented in Fig. 5 are the crystal length and width distributions obtained from the measurements of 'SPO A', 'SPO B' and 'SPO C' oxalate crystals. Equidistant 2.5 μm and 0.25 mm size intervals are used for the presentation of the crystal length and crystal width distributions, respectively. The measured length and width distributions show a significant difference in the geometry of the three types of oxalate crystals. As shown in Fig. 5(a), the 'SPO B' oxalate crystals exhibit the narrowest crystal length distribution and the smallest mean crystal length. In contrast, the "SPO C" oxalate crystals show a very broad crystal length distribution and the largest mean crystal length. On the other hand, the SPO A crystals display the narrowest width distribution and the smallest mean crystal width, as shown in Fig. 5(b).

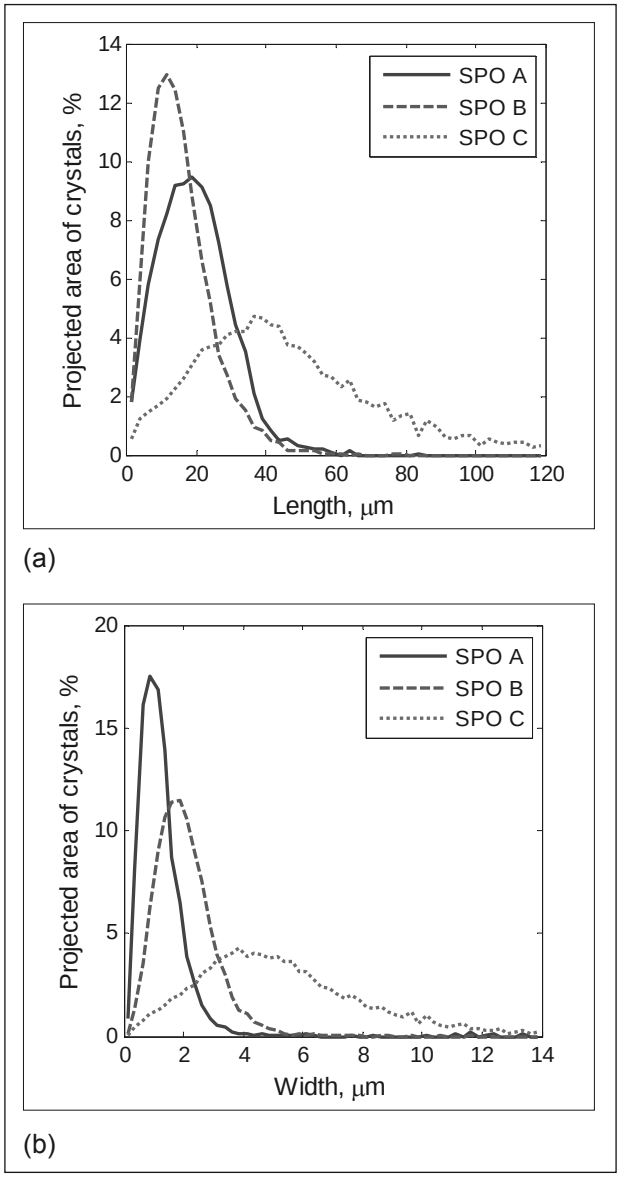

Fig. 5: Projected area-based length (a) and width (b) crystal distributions for three different types of oxalate crystals.

The corresponding crystal aspect ratio distributions are shown in Fig. 6. Both, number-based and projected area-based aspect ratio distributions are similar for 'SPO C' and 'SPO B' crystals, with 'SPO A displaying a different, narrower, aspect ratio distribution.

The maximum of aspect ratio distribution for 'SPO A' oxalate crystals is located at a smaller aspect ratio value than those for 'SPO B', and 'SPO C' crystals. It means that on average 'SPO A' oxalate crystals are more elongated than 'SPO B' and 'SPO C' crystals. In spite of the similarity between the 'SPO B', and 'SPO C' aspect ratio distributions, the length and width distributions of the two types of oxalate crystals differ significantly, as shown in Fig.5. This clearly illustrates the lack of sensitivity of the aspect ratio parameter for identifying differences between the crystals of different type.

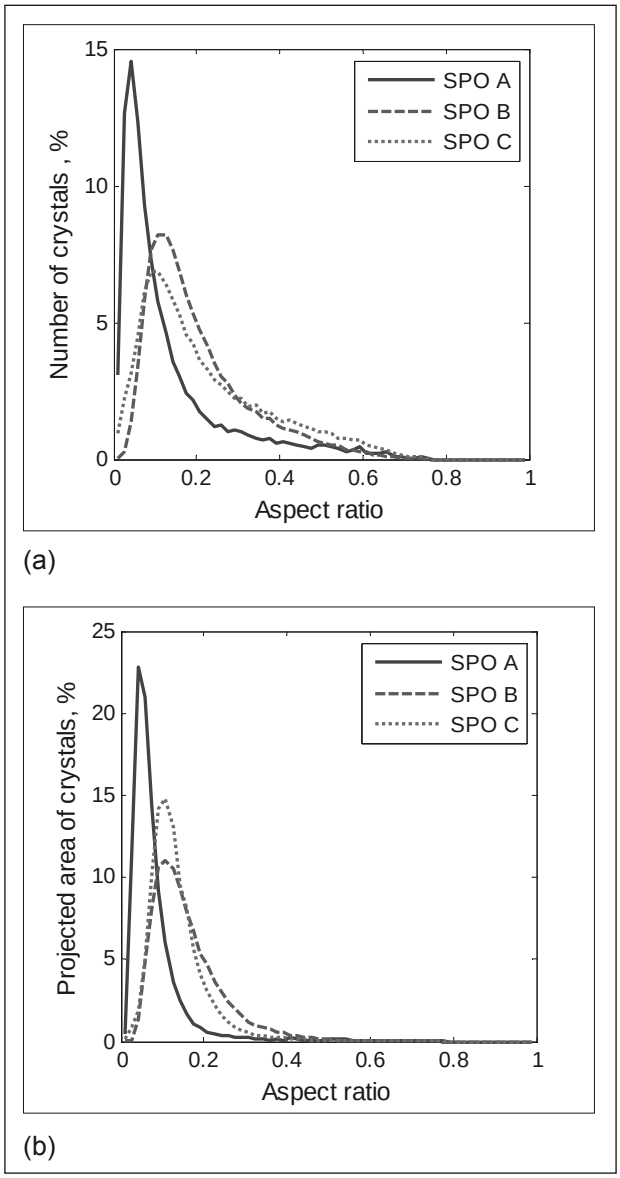

Fig. 6: Number-based aspect ratio distributions (a), and projected area-based aspect ratio distributions (b) for three different types of oxalate crystals.

Table 1 shows the number of crystals identified by the image analysis for each type of SPO crystals. Note that a higher number of crystals had to be identified in the case of 'SPO B' and 'SPO C' samples because of their broader aspect ratio distributions, as discussed by Bekker *et al.*, (2011). The number of rejected particles was highest in the case of 'SPO B' crystals. The estimated SSA shows the same trend as the measured SSA obtained by the BET method. Although the two values for low surface area SPO are very close, the deviation between the estimated and measured SSA becomes larger for more elongated, low aspect ratio, crystals such as 'SPO A'. For comparison, SEM images of two oxalate crystal samples, 'SPO A' and 'SPO C' are shown in Fig.7.

Table 1. Data from image analyses of different types of oxalate crystals.

Sample Name	Raw Number of Crystals	Number of Indentified Crystals	Rejected Crystals, %	Estimated SSA, m^2/g	Measured SSA, m^2/g
SPO A	42,093	36,267	13.86	1.2	4.0
SPO B	111,808	87,567	21.68	0.90	1.7
SPO C	93,256	81,983	12.09	0.31	0.41

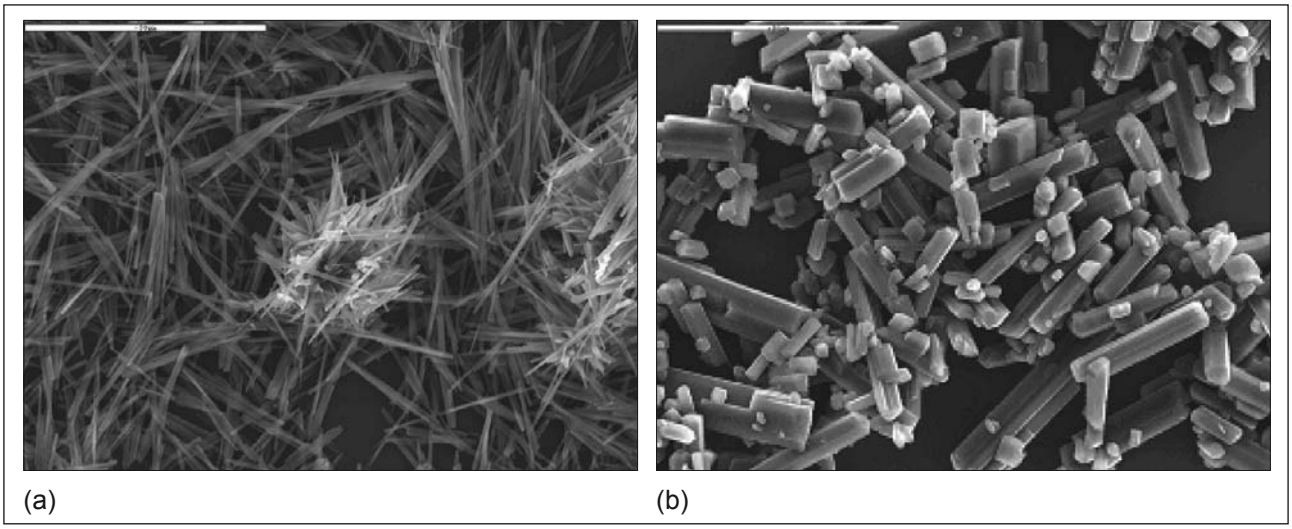

Fig. 7. SEM images of laboratory prepared oxalate crystals: (a) 'SPO A', and (b) 'SPO C'.

5. Validation of image analysis results against AccuSizer measurements

Results from the developed image analysis sizing method can be converted into a 1-D form suitable for comparison against a laser light extinction sizing instrument, Accusizer 780AD (Audet *et al.*, 2005). The Accusizer instrument is used to determine a number-based crystal size distribution over a large dynamic range, from 0.5 to 400 mm. Reproducibility of the AccuSizer oxalate crystal size distribution results was assessed by repeated measurements of the 'SPO A' crystals. Results from multiple AccuSizer measurements of 'SPO A', shown in Fig.8(a), indicate very good reproducibility of crystal size distribution measurements, with uncertainties only starting to increase once the number of crystals is reduced below 0.1% of the maximum number counted. Standard geometrical AccuSizer size intervals were used for plotting number-based crystal size distributions, as shown in Fig.8 and Fig.9.

As a light extinction-based instrument, the AccuSizer evaluates the characteristic crystal size in terms of the equivalent circle diameter. For the purpose of comparison to AccuSizer data, the projected area of crystals obtained by the SOIA technique was also converted to the diameter of an equivalent-area circle using the expression in Eq.1. In Fig.8(b), the SOIA generated crystal size distributions, raw and filtered, are compared to that obtained by the AccuSizer. Overall, a reasonably good agreement between the two techniques can be observed. The agreement is very good in the lower size range of the crystal size distribution, but starts deteriorating in the larger crystal size range, where the AccuSizer distribution typically falls in between the raw and filtered SOIA distributions. This may indicate that in some instances the AccuSizer detects crystal clusters rather than individual crystals, resulting in a larger then expected apparent crystal size.

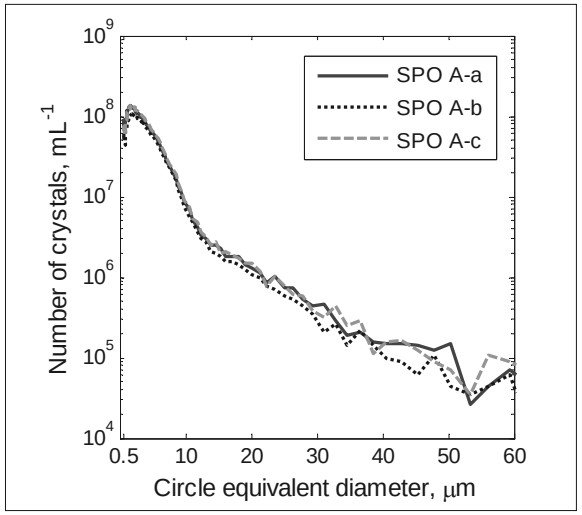

Fig. 8. Repeated AccuSizer measured number-based 'SPO A' crystal size distributions (a), and AccuSizer and SOIA number-based 'SPO A' crystal size distributions (b).

Comparisons between the AccuSizer and SOIA crystal size distributions for 'SPO B' and 'SPO C' samples are shown in Fig.9(a) and (b). Similar to the 'SPO A' case, a relatively good agreement between the two techniques is exhibited, therefore confirming the consistency of the results obtained by the new SOIA measuring technique.

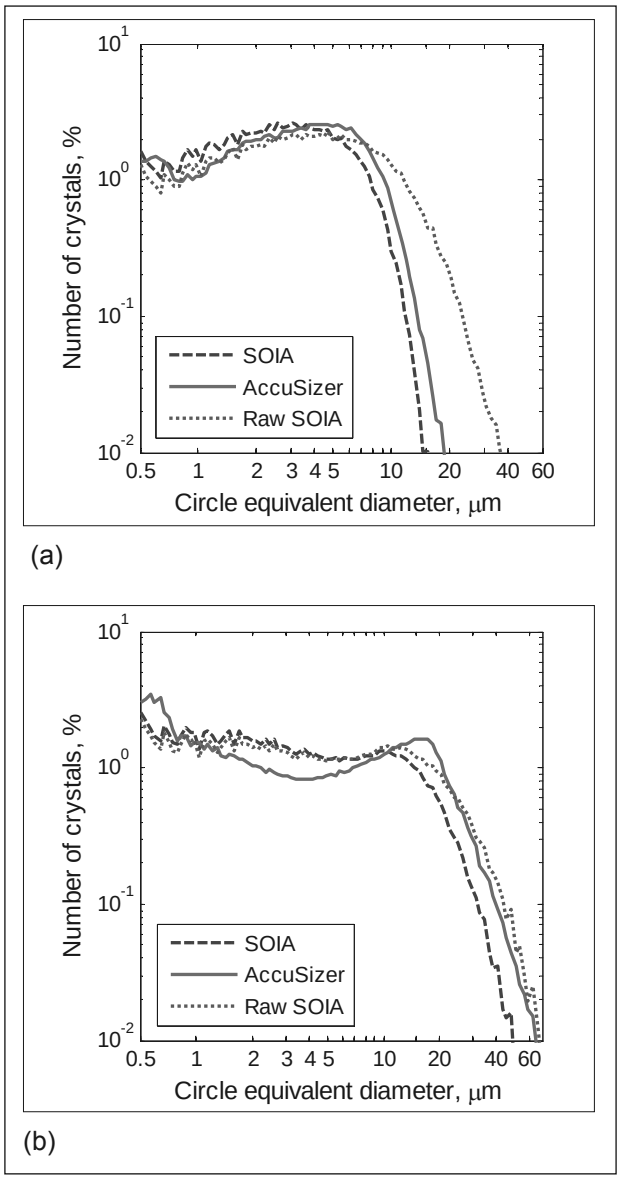

Fig. 9: AccuSizer and SOIA number-based crystal size distributions for: (a) 'SPO B' crystals, and (b) 'SPO C' crystals.

Possible reasons for the differences observed between the AccuSizer and SOIA size distributions can be summarised as: i) possible preferential SOIA morphological filtering of larger crystals, ii) clustering of SPO crystals during AccuSizer measurements, and iii) possible random orientation of crystals within the AccuSizer optical path.

6. Conclusions

The newly developed static optical image analysis (SOIA) technique for measuring the shape of sodium oxalate crystals overcomes many difficulties of classical sizing techniques by separately measuring the length and width of individual oxalate crystals. The SOIA technique combines automated acquisitioning of oxalate crystal images and a custom-developed numerical algorithm for crystal image identification and morphological analysis of detected crystals. The automation of the two main measuring steps enables characterisation of a large number of oxalate crystals ensuring statistically meaningful results. As part of the numerical algorithm, a specialised non-dimensional morphological filter was designed to eliminate overlapping crystals and crystal networks. This optical sizing technique has a low detection limit of 0.25 μm, which is close to the theoretical resolution of optical microscopy.

In this work, samples of three different types of oxalate crystals were measured to successfully demonstrate the high sensitivity of the SOIA technique to identify oxalate crystals of different shape. The optical image analysis-based measurements of SPO crystals were compared to those obtained by the AccuSizer sizing instrument to confirm that they were consistent with the results obtained by a conventional commercially available crystal sizing instrument.

References

Alcoa Newsletter, 2010, http://www.alcoa.com/australia/en/info_page/newsletter_201009_2.asp

Audet, DR, Rossiter, DS, & Sipos, G., 2005, 'Evaluation of number based particle size analysers', *Proceedings of the 7th International Alumina Quality Workshop*, Perth, Australia, 16-21 October.

Bekker AV, McShane J, Bedell D & Livk I, 2011, 'Image Analysis-based Sizing of Oxalate Crystals', *CD-ROM Proceedings of the Chemeca 2011 Conference*, Sydney, Australia, 18-21 September, 10 pages.

Darakis, E, Khanam, T, Rajendran, A, Kariwala, V, Naughton, T J & Asundi, A K 2010, 'Microparticle characterization using digital holography', *Chemical Engineering Science,* vol. 65, no. 2, pp. 1037-1044.

Ferreira, A, Faria, N, Rocha, F & Teixeira, JA, 2011, 'Using an Online Image Analysis Technique to Characterize Sucrose Crystal Morphology during a Crystallization Run', *Industrial & Engineering Chemistry Research,* vol. 50, no. 11, pp. 6990–7002.

Grocott, S C, 1988, 'Bayer liquor impurities: measurement of organic carbon, oxalate and carbonate extraction from bauxite digestion', *Light Metals*, pp. 833-841.

ISO 13322-2:2006. Particle size analysis – Image analysis methods — Part 2: Dynamic image analysis methods.

Khanam, T, Rahman, M N, Rajendran, A, Kariwala V & Asundi, A K 2011, 'Accurate Size Measurement of Needle-shaped Particles using Digital Holography', *Chemical Engineering Science*, vol. 66, no.12, pp. 2699-2706.

Larsen, P A, Rawlings, J B & Ferrier, N J, 2006, 'An algorithm for analyzing noisy, in situ images of high-aspect-aspect ratio crystals to monitor particle size distribution', *Chemical Engineering Science,* vol. 61, no. 16, pp. 5236–5248.

Lever, G 1983, 'Some aspects of the chemistry of bauxite organic matter on the Bayer process: the sodium oxalate-humate interaction', *Travaux*, vol. 13, no. 18, pp. 335-347.

Li, R F, Thomson, G B, White, G, Wang, X Z, De Anda, J C & Roberts, K J, 2006, 'Integration of crystal morphology modeling and on-line shape measurement', *AIChE Journal*, vol. 52, pp. 2297–2305.

Power, G P, 1991, 'The impact and control of organic compounds in the extraction of alumina from bauxite'. *Proceedings of the Fifth AusIMM Extractive Metallurgy Conference*, Perth, Australia, 2-4 October, pp. 337-334.

Rao, K V & Goyal, R N, 2006, 'Organic carbon in indian bauxites and its control in alumina plants', *Proceedings of 2006 TMS Annual Meeting Light Metals*, San Antonio, Texas, USA, March 12-16, pp. 71-74.

Rehani, M, Dwyer, A, Parkinson, G, Rosenberg, S P, Healy, S J, Armstrong, L, Soirat, A & Rowe, S, 1999, 'Gibbsite nucleation at sodium oxalate surfaces', *Proceedings of the 5th International Alumina Quality Workshop,* Bunbury, Australia, 21-26 March, p. 181.

Sipos G, 2001, 'The mechnism and action of sodium oxalate seed stabilizer molecules under Bayer conditions', *PhD Thesis, School of Applied Chemistry, Curtin University of Technology*, Australia, 161 pages.

Wang, X Z, Calderon De Anda, J & Roberts, K J, 2007, 'Real-time measurement of the growth rates of individual crystal facets using imaging and image analysis: a feasibility study on needle-shaped crystals of L-glutamic acid', *Trans of IChemE Part A: Chemical Engineering Research and Design*, vol. 85, no. A7, pp. 921-927.

Zaknich, A & Attikiouzel, Y, 1995, 'Detection of Sodium Oxalate Needles in Optical Images Using Neural Network Classifiers'. *1995 IEEE International Conference on Neural Networks*, Perth, vol. 4, pp. 1699-1702.